






Resolving Massive Black Hole Binary Evolution via Adaptive Particle Splitting

Alessia Franchini^{1,2} , Alessandro Lupi¹ , and Alberto Sesana¹ ¹ Dipartimento di Fisica “G. Occhialini”, Università degli Studi di Milano-Bicocca, Piazza della Scienza 3, I-20126 Milan, Italy; alessia.franchini@unimib.it² INFN, Sezione di Milano-Bicocca, Piazza della Scienza 3, I-20126 Milano, Italy

Received 2021 December 5; revised 2022 February 25; accepted 2022 April 3; published 2022 April 12

Abstract

The study of the interaction of a massive black hole binary with its gaseous environment is crucial in order to be able to predict merger rates and possible electromagnetic counterparts of gravitational-wave signals. The evolution of the binary semimajor axis resulting from this interaction has been recently debated, and a clear consensus is still missing because of several numerical limitations, i.e., fixed orbit binaries or lack of resolution inside the cavity carved by the binary in its circumbinary disk. Using on-the-fly particle splitting in the 3D meshless code GIZMO, we achieve hyper-Lagrangian resolution, which allows us to properly resolve the dynamics inside the cavity—in particular, for the first time, the disks that form around the two components of a live binary surrounded by a locally isothermal gaseous circumbinary disk. We show that the binary orbit decays with time for very cold and very warm disks and that the result of the interaction in the intermediate regime is strongly influenced by the disk viscosity, as this essentially regulates the fraction of mass contained in the disks around the binary components, as well as the fraction that is accreted by the binary. We find the balance between these two quantities to determine whether the binary semimajor axis decreases with time.

Unified Astronomy Thesaurus concepts: [Stellar accretion disks \(1579\)](#); [Accretion \(14\)](#); [Hydrodynamical simulations \(767\)](#); [Binary stars \(154\)](#); [Black holes \(162\)](#)

1. Introduction

Massive black holes (MBHs) are expected to reside in the nuclei of (virtually all) massive galaxies (e.g., Kormendy & Ho 2013). When two massive galaxies merge, the MBHs in their centers migrate toward the center of the newly formed galaxy owing to the effect of dynamical friction (Chandrasekhar 1943) against the background of stars and gas. The two MBHs are expected to form a bound MBH binary (MBHB) at parsec scales. At these scales, dynamical friction becomes inefficient, and further evolution of the binary orbit toward coalescence requires a mechanism to extract angular momentum and energy from the binary. The main mechanisms proposed in the literature are three-body scattering of stars intersecting the binary orbit (e.g., Quinlan 1996; Sesana et al. 2007) or the interaction with a circumbinary gaseous disk (Escala et al. 2005; Dotti et al. 2007; Cuadra et al. 2009), depending on the binary separation scale (see Bortolas et al. 2021 for details on the competition between stellar and gaseous interaction).

Each of the two massive galaxies brings with it a significant amount of gas that sinks to the center, forming a circumbinary accretion disk. This gaseous disk might facilitate the MBHB merger and give rise to electromagnetic counterparts of the gravitational-wave (GW) emission (Begelman et al. 1980; Armitage & Natarajan 2002; Lodato et al. 2009). A coplanar accretion disk can extend down to a few times the binary separation (Artymowicz & Lubow 1994). The disk orbits resonate with the binary orbit at discrete locations (outer Lindblad resonances), leading to the exchange of angular momentum between the disk and the binary (Lynden-Bell & Kalnajs 1972; Lin & Papaloizou 1986). The magnitude of the

resonant torques depends on the binary potential, i.e., its mass ratio and eccentricity, and is proportional to the disk surface density at the resonance locations (Goldreich & Tremaine 1979). Therefore, the amount of angular momentum transferred from the binary to the disk at the resonances depends on the disk properties as well.

Very early numerical simulations (Artymowicz & Lubow 1994, 1996) investigated the interaction of a binary with its gaseous circumbinary disk, finding that only a small amount of material is able to enter the cavity carved by the binary and accrete onto the binary components. The main finding of these works is that the binary semimajor axis decreases with time owing to the interaction with the disk. This picture has been recently challenged by a few works (Muñoz et al. 2019; Duffell et al. 2020; Muñoz et al. 2020) employing 2D (and one 3D; see Moody et al. 2019) static or moving-mesh grid numerical simulations with fixed binary orbits. In particular, these studies found that the secular angular momentum transfer onto the binary is strongly positive within the range of binary and disk parameters explored. More recently, Tiede et al. (2020) found, using the same numerical techniques, that the sign of the torque exerted by the disk onto the binary depends on the disk temperature, i.e., its aspect ratio H/R , for locally isothermal disks. In particular, they found disks with $H/R \lesssim 0.04$ to shrink the binary. Using 3D smoothed particle hydrodynamics (SPH) simulations of locally isothermal disks, Heath & Nixon (2020) instead found the threshold value for binary expansion to be $H/R \simeq 0.2$. Other works that employed SPH simulations in the regime where the disk self-gravity cannot be neglected and the disk temperature changes with time found binary shrinking as a result of the interaction with massive disks regardless of the disk temperature (Cuadra et al. 2009; Roedig et al. 2012; Franchini et al. 2021). The discrepancy in the results inferred using different numerical techniques has been argued to originate from the lack of numerical resolution in SPH simulations, which, in contrast with grid-based ones,



Original content from this work may be used under the terms of the [Creative Commons Attribution 4.0 licence](#). Any further distribution of this work must maintain attribution to the author(s) and the title of the work, journal citation and DOI.

were unable to properly resolve the dynamics of the gas streams entering the cavity, artificially suppressing the positive torque associated with such gas that forces the binary to expand (Muñoz et al. 2019).

In this letter, we employ the public version of the code GIZMO (Hopkins 2015) in its meshless finite mass (MFM) mode coupled with adaptive particle splitting for numerical refinement of the gas dynamics inside the disk cavity, with the aim of accurately measuring the gravitational and accretion torques that originate from the disks that form around the binary components (also called *minidisks*) onto the binary itself.³

In Section 2, we describe the details of the numerical method and present the results of our simulations in Section 3. We discuss the relevance of the parameters explored in Section 4 and finally draw our conclusions in Section 5.

2. Numerical Setup

The initial conditions for this work consist of a live binary surrounded by a circumbinary gaseous disk. The 3D distribution of the 10^6 equal-mass gas particles sampling the disk and the initial orbit of the two sink particles of the binary are generated using the SPH code PHANTOM (Price et al. 2018). The equal-mass binary has an initial mass $M = M_1 + M_2 = 1$ and a separation $a = 1$. The circumbinary disk initially extends from $R_{\text{in}} = 2a$ to $R_{\text{out}} = 10a$, with a fixed aspect ratio $H/R = 0.1$. The gas is described by a locally isothermal equation of state with the sound speed c_s defined by Equation (4) in Farris et al. (2014) and a surface density profile scaling as $\Sigma \propto R^{-3/2}$, normalized to get a total mass $M_{\text{disk}} = 0.1M$.

The simulations are performed with the MFM method in GIZMO, keeping the binary live; i.e., its orbit is allowed to change during the evolution. The MFM is a mesh-free Lagrangian approach that encapsulates the advantages of both grid- and particle-based codes. In particular, by partitioning the domain with discrete tracers (particles/cells) and solving the integral form of the fluid dynamics equations via a finite-volume Godunov method, this numerical technique allows one to obtain intrinsic adaptivity in resolution while minimizing the numerical advection of angular momentum through the “cells” and also ensures shock capturing without the need of the extra artificial viscosity terms commonly used in SPH codes. Here we also include the effect of gas viscosity entering the Navier–Stokes fluid equations as described in Hopkins (2016), assuming a shear viscosity in the disk $\nu = \alpha c_s H$ parameterized using a viscosity parameter $\alpha = 0.1$ (Shakura & Sunyaev 1973) and no bulk viscosity.

2.1. Gas Accretion and Gravitational Forces

Every time a gas particle approaches one of the sinks, entering its sink radius r_{sink} , we flag it as eligible to be accreted. During the accretion event, conservation of mass and linear and angular momentum are ensured in the same way as in the PHANTOM code (Bate et al. 1995).⁴ In this work, we neglect the

disk self-gravity and only include the gravitational interaction between (i) the two sink particles and (ii) the sink and gas particles (see Franchini et al. 2021, for a discussion about the role of self-gravity). In order to get a high accuracy in the dynamical evolution, we suitably modify the code as follows. First, we include the gravitational acceleration exerted by the gas particles onto the two black holes via direct summation, which guarantees the most accurate estimation of the acceleration on both sinks. Second, we introduce a new time-step criterion for the sink particles that forces both of them to evolve on the shortest common time step. Finally, we reset the center of mass and the center-of-mass velocity of the entire system to the origin at each course time step in order to avoid the buildup of small conservation errors in the linear momentum that, over the long integration times we consider, might displace the binary from the center. Note that this does not influence the dynamics of the system, since it simply corresponds to a rigid shift of the positions and velocity of the center of mass of all sink and gas particles to the origin.

2.2. Particle Splitting

In order to increase the resolution when and where necessary without globally slowing down our simulations, we employ an on-the-fly adaptive particle-splitting approach, which is similar in spirit to the adaptive mesh refinement of grid-based codes. Such a technique represents a natural generalization of the refinement/de-refinement scheme in AREPO (Springel 2010) and GIZMO (Hopkins 2015) to maintain an almost constant mass per cell during the simulations when a finite-volume scheme is employed. In this work, we exploit the particle-splitting algorithm in GIZMO, splitting gas particles that enter a sphere of radius r_{ref} centered on the center of mass of the binary–disk system. In particular, particles at radii $r < r_{\text{ref}}$ are split when their mass $m \gtrsim \chi_{\text{ref}} m_{\text{max}}$, where m_{max} is a scale mass and χ_{ref} is the refinement factor, a suitably defined function, which we choose of the form

$$\chi_{\text{ref}}(r) = \begin{cases} \chi_{\text{ref}}^{\text{min}} & \xi < \xi_{\text{min}} \\ A\xi^2 + B\xi + C & \xi_{\text{min}} \leq \xi \leq \xi_{\text{ref}} \\ 1 & \xi > 1 \end{cases} \quad (1)$$

Here $\xi = r/r_{\text{ref}}$, $\xi_{\text{min}} = r_{\text{min}}/r_{\text{ref}}$ with r_{min} the radius at which the maximum resolution is reached, $\chi_{\text{ref}}^{\text{min}} = 1/32$, and the coefficients are defined as $A = (1 - \chi_{\text{ref}}^{\text{min}})/(1 - \xi_{\text{min}})^2$, $B = -2A\xi_{\text{min}}$, $C = 1 - A(1 - 2\xi_{\text{min}})$. In particular, we choose $r_{\text{min}} = 0.75a$, which guarantees that the flow around the two components of the binary is always at the maximum resolution, and $r_{\text{ref}} = 4a$, which allows one to properly resolve the edge of the cavity and the dynamics of the gas streaming inward.

When a particle is flagged for refinement, two children are created, each with mass $0.5m$ and located at a distance $dr = \min(0.25h, 0.35d_{\text{nbg}})$, where h is the particle kernel size and d_{nbg} is the distance to the nearest neighbor, from the position of the parent and on opposite sides along a random direction. The numerical factors are necessary to minimize perturbations to hydrodynamic quantities and avoid overlapping of fluid elements (Anglés-Alcázar et al. 2020). All of the remaining properties are instead directly inherited by the children. This approach allows the almost perfect conservation of momentum, angular momentum, and energy throughout the simulation. The density is recalculated immediately after the

³ The adaptive particle-splitting technique has been previously successfully employed in isolated (Curtis & Sijacki 2015) and cosmological (Anglés-Alcázar et al. 2020) simulations to resolve the dynamics of the gas as it approaches the central MBH.

⁴ Note that in the public implementation of the accretion in GIZMO, the linear momentum conservation only accounts for the change in the center-of-mass position and velocity, neglecting the acceleration term (see Price et al. 2017, for details). Since this has the effect of reducing the momentum conservation accuracy, which is crucial in our study, we suitably added it to the code.

splitting using the standard approach. In addition to splitting, particles are also allowed to merge when their mass is significantly below the resolution requirements, i.e., $m < \chi_{\text{ref}} m_{\text{min}}$, with m_{min} the scale mass for the merger. In our numerical simulations, we set m_{max} equal to the initial mass of the particles in the disk and m_{min} to 1/1000 of it, which translates into neglecting merging, although we also explored different values and the inclusion of mergers, finding negligible differences.

3. Results

We now describe our main results, exploring how different parameters and resolution requirements affect our conclusions.

3.1. Lagrangian Resolution

As a first check of our numerical and physical setup, we performed a simulation using standard Lagrangian resolution, i.e., switching off particle splitting, and a large sink radius $r_{\text{sink}} = 0.2$ in order to obtain a fair comparison with the results presented in Heath & Nixon (2020). We find a general agreement between our simulation with $H/R = 0.1$ and that represented by the red dashed curve in Figure 4 of Heath & Nixon (2020), with the binary shrinking over time. We also performed the same test with a thicker disk, i.e., $H/R = 0.2$, in this case finding binary expansion, as already found by Heath & Nixon (2020).

We note that the rate at which the binary shrinks (or expands) is in general slightly higher in our runs than in Heath & Nixon (2020), likely because of the different treatment of hydrodynamics (e.g., different numerical treatment of shocks) in the two codes and the slightly different equation of state employed for the gas. However, a precise comparison between the codes is beyond the scope of this work.

3.2. Hyper-Lagrangian Resolution

The use of pure Lagrangian resolution has been argued to possibly lead to a less accurate treatment of the interaction between a binary and its circumbinary disk because of the small amount of particles entering the cavity, resulting in a poor resolution around the two MBHs. In order to overcome this potential limitation, here we employ on-the-fly particle splitting, which allows us to significantly increase the resolution of our simulations in the cavity at a moderate computational cost.

Here we show and discuss the result of our fiducial case with particle splitting (implemented according to Equation (1)); disk aspect ratio $H/R = 0.1$, constant throughout the disk; and viscosity parameter $\alpha = 0.1$. Compared to the purely Lagrangian tests, the sink size is now reduced to $r_{\text{sink}} = 0.05$ to ensure that the gas dynamics around each MBH is properly resolved.

Figure 1 shows the column density plots of the circumbinary disk, together with the resolved disks around the two binary components (white circles) obtained with particle splitting at $t = 500, 1500, 2000, 2500 P_b$. We can clearly resolve the dynamics inside the cavity carved by the live binary using our hyper-Lagrangian approach. The cavity does not remain circular, as already observed in previous studies (Ragusa et al. 2016; Muñoz et al. 2019; Heath & Nixon 2020), and the formation of shocks at the cavity edge is also expected due to the part of the streams that gets flown back to the disk inner edge after entering the cavity.

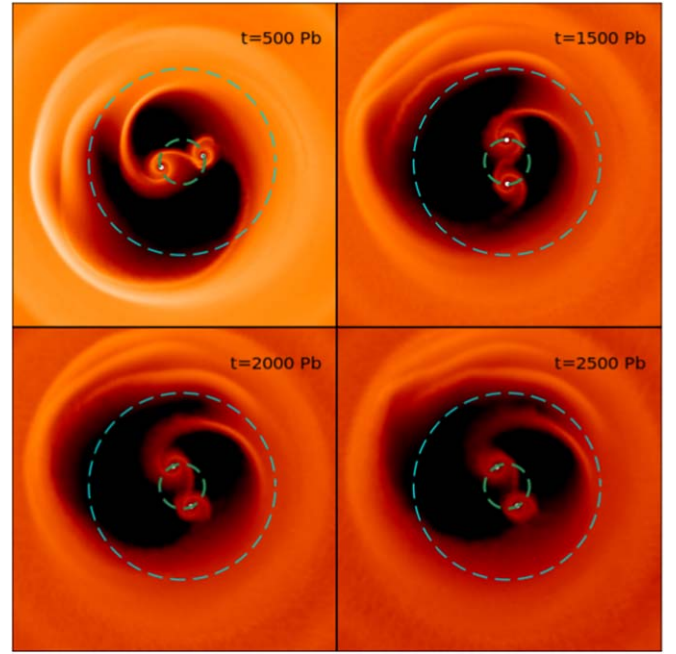


Figure 1. Column density plots of the circumbinary disk and the disks around the binary components (shown by the white circles). The view is of the x - y plane (i.e., the binary orbital plane), and the density has been integrated through z . The color scale spans about 3 orders of magnitude in density and is the same for all plots. The green dashed circle corresponds to the initial binary orbit, and the cyan dashed circle corresponds to the location of the strongest Lindblad resonance, i.e., $2.08a$.

We test the conservation of angular momentum in the simulations with and without particle splitting, following the procedure outlined in Franchini et al. (2021; see also Muñoz et al. 2019), in order to ensure that the particle-splitting algorithm does not significantly affect the conservation. We divide the contribution of the disk to the change in the binary angular momentum into a gravitational and an accretion part, the latter including the fraction of the accreted angular momentum that is converted into the spin of the two MBHs.

The left panel of Figure 2 shows the contributions to the binary angular momentum change as computed directly from our fiducial simulation. In particular, from the comparison between the black solid line (i.e., the sum of the gravitational and accretion contribution) and the red line that shows the live binary angular momentum change, it is evident that the angular momentum is conserved in our fiducial run almost exactly. The small discrepancy is due to our approximate calculation of the gravitational torque between two subsequent snapshots instead of calculating it at each time step. As a further consistency check, we also compared the same quantities in a simulation without particle splitting (keeping $r_{\text{sink}} = 0.05$), finding the impact of the refinement scheme on the conservation to be negligible.

Since the simulation conserves angular momentum, we can write the evolution of the binary semimajor axis as

$$\frac{\dot{a}}{2a} = \frac{\dot{L}_{z,\text{acc}}}{L_z} + \frac{\dot{L}_{z,\text{grav}}}{L_z} - \frac{\dot{\mu}}{\mu} - \frac{\dot{M}}{2M} + \frac{e\dot{e}}{(1-e^2)}, \quad (2)$$

where $L_z = \mu\sqrt{GMa(1-e^2)} = L_{z,\text{grav}} + L_{z,\text{acc}}$ is the z component of the binary angular momentum, μ is the reduced mass, and e is the binary eccentricity. The first term is always positive and represents the accretion of angular momentum

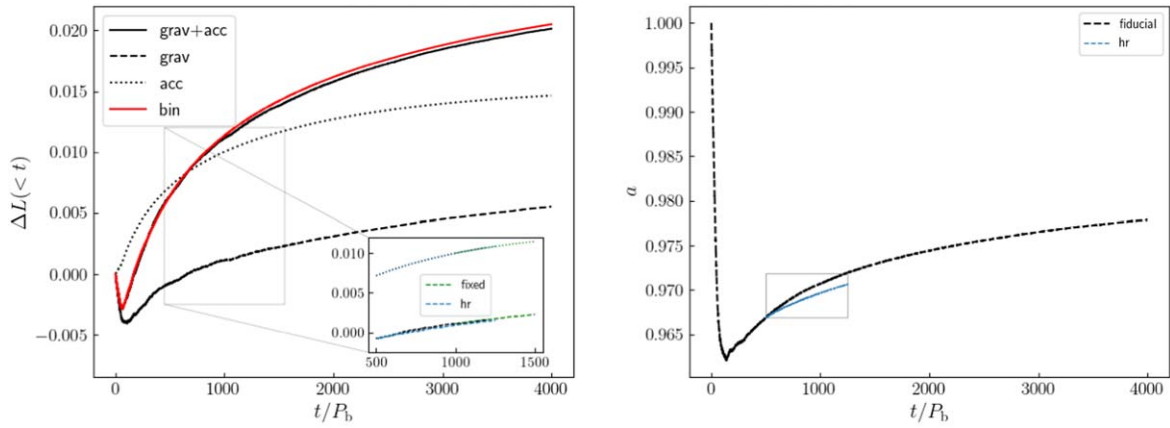


Figure 2. Left panel: conservation of angular momentum in our fiducial run with particle splitting. The dotted and dashed curves show the cumulative contribution of mass accretion and gravity, respectively, and the black solid line is the sum of the two. The red line shows the evolution of the angular momentum of the live binary. The inset shows the accretion (dotted line) and gravitational (dashed line) torques measured from our fixed binary orbit (green) and high-resolution (blue) run. Right panel: evolution of the binary semimajor axis with time in our fiducial (black line) and higher-resolution (blue line) run with particle splitting. The time is in units of the binary orbit period, i.e., $P_b = 2\pi$ in code units.

onto the binary (dotted line in Figure 2). The second term is given by the sum of the positive contribution of the disks around the two components and the negative contribution of the circumbinary disk and corresponds to the dashed line in Figure 2. The terms due to the accretion of mass (i.e., third and fourth terms) are additional negative contributions to the semimajor axis evolution. The last term comes from the binary eccentricity evolution, and we find it to be negligible in our runs. Therefore, we essentially have two positive terms whose effect is to drive the binary apart and two negative contributions that remove angular momentum from the binary, driving it toward merger. In more physical terms, the angular momentum change due to the gravitational and accretion torques translates into a change of the different elements of the system, i.e., the masses and orbital elements. Since the eccentricity contribution is negligible in our runs, the evolution of the binary separation depends on the fraction of the angular momentum exchanged with the disk that goes into the mass accretion terms.

The right panel of Figure 2 shows the evolution of the live binary semimajor axis with time, directly calculated from our fiducial run using energy and angular momentum conservation. The binary semimajor axis decreases within the first ~ 100 binary orbits due to a transient phase as the disk adjusts to an equilibrium configuration. After the first 100 orbits, the shape (and size) of the cavity changes significantly as the streams are flown back to the circumbinary disk. This causes the amount of material at the 2:1 Lindblad resonance (represented by the cyan dashed circle in Figure 1) to decrease by a factor of ~ 5 – 10 , weakening the strength of the resonance. As a consequence, the positive torque provided by the disks around the binary components, which is able to overcome the negative contribution of the circumbinary disk, leads to the increase of the binary separation.⁵ We find the expansion phase to be very mild and the semimajor axis to increase at a progressively slower pace. This might be due to the progressive decrease of the disk mass owing to accretion, which drops to $M_d \approx 0.04M$

after 4000 orbits. We note that this phase appears to be in broad agreement with the findings of grid code simulations (Muñoz et al. 2019; Duffell et al. 2020) indicating that, indeed, resolving the dynamics inside the cavity is important in order to properly investigate the binary–disk interaction.

3.3. The Impact of Spatial/Mass Resolution and Live/Fixed Binary Orbits

Although the extremely high resolution achieved owing to the hyper-Lagrangian refinement enabled us to better resolve the gas flowing into the cavity, it might be argued that the resolution achieved is insufficient to properly measure torques in the cavity. We have therefore estimated the average interparticle separation of the gas in the disks surrounding the binary components in our fiducial simulation, finding $\Delta r \approx 0.015a$. This corresponds to, e.g., the mid-resolution run in Tiede et al. (2020), already confirming the good accuracy of our measured torques. Nonetheless, we have further investigated the impact of resolution inside the cavity by decreasing the minimum refinement factor down to $\chi_{\text{ref}}^{\text{min}} = 1/64$, i.e., by a factor of 2. In order to avoid the initial transient in the orbital evolution, we have restarted our fiducial run from the 500th orbit, carefully emptying the cavity to prevent numerical instabilities arising from a sudden increase in resolution near the binary components. Note that the amount of mass removed by this process is negligible compared to the disk mass, and the removal does not affect the subsequent evolution, since the disks around the two components reform in less than one orbit. We find the structure and density of these disks to remain essentially unaltered and unaffected by the increase in resolution. The blue lines in the left panel inset of Figure 2 show the gravitational and accretion torque measured in this case. We find the accretion torque to remain the same, while the gravitational torque is slightly lower in this high-resolution run. This reflects on the evolution of the binary semimajor axis (see the blue line in the right panel inset in Figure 2), which increases at a slightly slower pace.

The majority of the previous studies of circumbinary disks are based on simulations in which the binary is kept on a fixed orbit. While this assumption might be reasonable when the change in binary properties is small, a proper analysis of its impact is in order. For this reason, we have also performed a

⁵ As a further check of our numerical setup, we ran a very high Lagrangian resolution (i.e., employing 10^7 SPH particles) simulation using the PHANTOM code, finding the same behavior as our fiducial run.

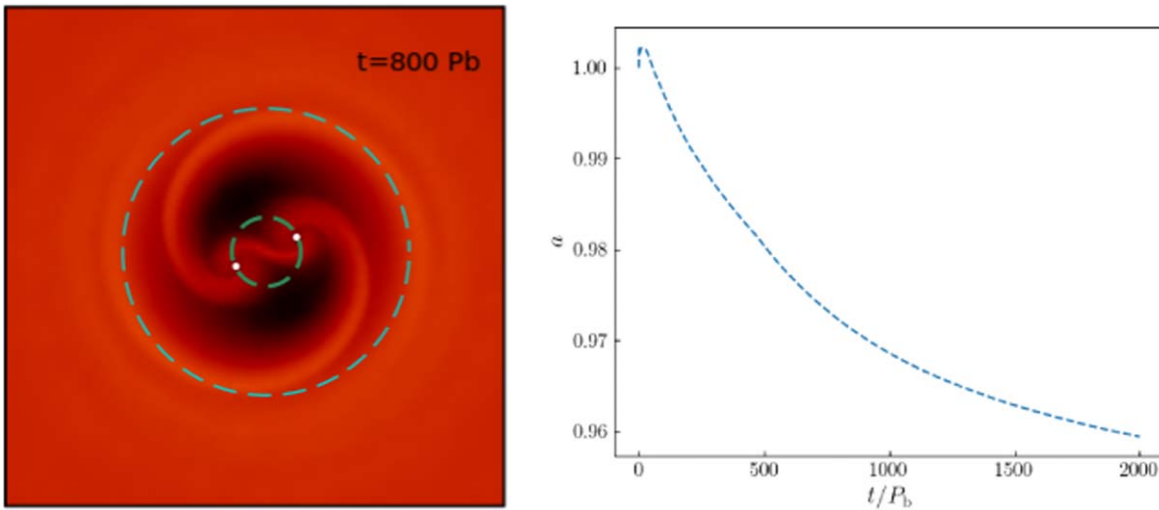


Figure 3. Left panel: same as Figure 1 but with $H/R = 0.2$ and shown at $t = 800P_b$. The density scale is the same as in Figure 1. Right panel: same as the right panel of Figure 2 but with a disk aspect ratio $H/R = 0.2$.

simulation identical to our fiducial run, in which we kept the binary orbit fixed, as in previous studies (Moody et al. 2019; Muñoz et al. 2019; Duffell et al. 2020). The comparison between the fixed and live binary orbit run, in terms of gravitational and accretion torques, is shown by the green lines in the left panel inset of Figure 2. We started the simulation from the 1000th binary orbit of our fiducial live binary run, since, by this time, the disk is in a quasi-steady state. We find that the accretion and gravitational torques do not vary significantly compared to our fiducial live binary simulation. We note, however, that the surface density of the disks that form around the two binary components is slightly lower in the simulation with a fixed binary orbit. This does not cause the torques to be significantly different over a few hundred orbits, but it is an effect that will be further analyzed in a future work.

3.4. Disk Temperature

In order to determine whether there is a critical condition that discriminates between binary shrinking and expansion, we also explored different disk temperatures, keeping the small sink radius $r_{\text{sink}} = 0.05$ and using particle splitting.

First, we decreased the disk aspect ratio to $H/R = 0.03$, i.e., within the regime where both grid code (Tiede et al. 2020) and SPH (Heath & Nixon 2020) simulations find binary shrinking, and we found our simulations with particle splitting to be in agreement with previous studies. We note that, given the low disk temperature, the mass in the disks around the binary components is very low, regardless of the refinement, and this reduces the positive contribution to the gravitational torque.

Heath & Nixon (2020) found, using pure SPH simulations without particle splitting, that circumbinary disks with aspect ratios $H/R \geq 0.2$ cause the binary orbit to expand, owing to the large amount of material that is able to enter the cavity and accrete onto the binary. For completeness and a further check for our fiducial run, we also explored the case of a thicker disk with $H/R = 0.2$.⁶

The left panel of Figure 3 shows the column density plots of the circumbinary disk, together with the resolved disks around

the two binary components (white circles) obtained with particle splitting for a thick accretion disk. The density scale is the same as in Figure 1. We find that the material that enters the cavity is significantly larger compared to the thinner disk simulation.

We can see from the right panel of Figure 3 that the binary semimajor axis decreases with time after undergoing a very brief and mild expansion within the first 20 orbits, even though the disk thickness is in the regime Heath & Nixon (2020) found for expansion. Despite the gravitational and accretion torques being positive throughout the duration of the simulation, we find that the negative contribution of the accretion of mass (and not angular momentum) dominates the evolution of the binary.

4. Discussion

Interestingly, we find that binary shrinks for thin and very thick disks and that there is a regime of intermediate disk thickness where the negative and positive torques balance out, leading to a phase of possible binary expansion.

We compared our simulation with $H/R = 0.1$ with and without particle splitting and found that having a small sink radius without resolving the disks that form around the binary components might result in an overestimate of the (positive) gravitational torque; this, in turn, leads to a much faster binary expansion phase. This lasts until the accretion of mass onto the binary components becomes large enough to overcome the positive torque and is very sensitive to the resolution inside the cavity. In our fiducial case, the expansion is significantly milder and slower; however, it seems to last for much longer due to the positive torque from the disks around the two components being strong enough to balance the negative torque from the accretion of mass. In our low-resolution simulation, we find that the binary semimajor axis decreases again after ~ 800 orbits. We further explored the effect of resolution by increasing the resolution inside the cavity by a factor of 2 with respect to our fiducial run. We find that our results are overall not affected by the numerical resolution.

The balance between the positive and negative torques is essentially regulated by the disk viscosity, which determines the amount of material that enters the cavity, forms the disks, and then accretes onto the binary components. Therefore,

⁶ Note that Heath & Nixon (2020) used a slightly different equation of state for the disk. In particular, their disk is flared, with $H/R(R_{\text{in}}) = 0.2$, while in our runs, the aspect ratio is constant throughout the disk.

different treatments and α values are very likely to change the binary evolution. For instance, decreasing the value of α by a factor of 2 in our fiducial run with aspect ratio $H/R = 0.1$ leads to the binary semimajor axis decreasing with time without transiting to the expansion phase.

Since the MFM method has been proven to give more accurate results on standard tests compared to the pure SPH approach (Hopkins 2015), even with a small number of neighbors, we reran our fiducial simulation with particle splitting but employing only 32 neighbors instead of the 58 used in the rest of this work. We find the expansion phase to be significantly milder.

We also note that, by $3500 P_b$, the binary in our fiducial run has already accreted $\sim 60\%$ of the initial disk mass, and the semimajor axis is still increasing, though at a progressively slower pace. In order to understand whether this phase is just a transient, in future work, we will implement gas particle injection to provide a constant source of gas into the circumbinary disk to feed the disks inside the cavity.

Finally, we do not find binary expansion in the simulation presented in Section 3.4 with $H/R = 0.2$ using particle splitting with a small accretion radius. The reason for this change resides in the gas distribution in the cavity. The gas distribution inside the disks around the binary components in the thicker disk case is uniform; therefore, removing the inner regions by enlarging the accretion radius leads to a higher specific angular momentum being transferred to the binary during accretion, which, in turn, causes the binary to expand. Although whether a threshold exists for binary expansion in terms of the disk aspect ratio still remains to be determined, such large disk thicknesses are well beyond the typical aspect ratio we may expect for circumbinary disks surrounding MBHBs, if their structure resembles that of active galactic nucleus disks (Collin-Souffrin & Dumont 1990).

5. Conclusions

In this work, we use hyper-Lagrangian refinement to resolve for the first time the gas dynamics inside the cavity carved by a live binary in its circumbinary disk using 3D hydrodynamical simulations employing the meshless finite mass numerical algorithm of the code GIZMO. In particular, resolving the disks that form around the binary components allows us to better measure the torques they exert on the binary. We find the gravitational torques by these disks to be positive, in broad agreement with the results of previous grid-based simulations (Muñoz et al. 2019; Duffell et al. 2020). However, we find that these are not strong enough to overcome the negative circumbinary disk torque and the negative angular momentum variation due to the accretion of mass in the cases of both thin and very thick disks.

We therefore conclude that the binary semimajor axis typically decreases with time as a result of the interaction with the gaseous accretion disk if the disk is thin, but even if the disk is very geometrically thick. Interestingly, we find an intermediate regime where the positive torque exerted by the disks around the binary components is able to counterbalance the

negative torques, leading to a possibly temporary phase of expansion. However, we caution that this is very sensitive to the viscosity treatment and therefore worth investigating more in detail in a follow-up paper.

We thank Daniel Price for providing the PHANTOM code for numerical simulations and acknowledge the use of SPLASH (Price 2007) for the rendering of the figures. We thank Phil Hopkins for providing the GIZMO code for numerical simulations. A.F. and A.S. acknowledge financial support provided under the European Union’s H2020 ERC Consolidator Grant “Binary Massive black hole Astrophysics” (B Massive, Grant Agreement: 818691). A.L. acknowledges funding from MIUR under grant PRIN 2017-MB8AEZ.

ORCID iDs

Alessia Franchini  <https://orcid.org/0000-0002-8400-0969>
Alessandro Lupi  <https://orcid.org/0000-0001-6106-7821>
Alberto Sesana  <https://orcid.org/0000-0003-4961-1606>

References

- Anglés-Alcázar, D., Quataert, E., Hopkins, P., et al. 2020, *ApJ*, 917, 53
Armitage, P. J., & Natarajan, P. 2002, *ApJL*, 567, L9
Artymowicz, P., & Lubow, S. H. 1994, *ApJ*, 421, 651
Artymowicz, P., & Lubow, S. H. 1996, *ApJL*, 467, L77
Bate, M. R., Bonnell, I. A., & Price, N. M. 1995, *MNRAS*, 277, 362
Begelman, M. C., Blandford, R. D., & Rees, M. J. 1980, *Natur*, 287, 307
Bortolas, E., Franchini, A., Bonetti, M., & Sesana, A. 2021, *ApJL*, 918, L15
Chandrasekhar, S. 1943, *ApJ*, 97, 255
Collin-Souffrin, S., & Dumont, A. M. 1990, *A&A*, 229, 292
Cuadra, J., Armitage, P. J., Alexander, R. D., & Begelman, M. C. 2009, *MNRAS*, 393, 1423
Curtis, M., & Sijacki, D. 2015, *MNRAS*, 454, 3445
Dotti, M., Colpi, M., Haardt, F., & Mayer, L. 2007, *MNRAS*, 379, 956
Duffell, P. C., D’Orazio, D., Derdzinski, A., et al. 2020, *ApJ*, 901, 25
Escala, A., Larson, R. B., Coppi, P. S., & Mardones, D. 2005, *ApJ*, 630, 152
Farris, B. D., Duffell, P., MacFadyen, A. I., & Haiman, Z. 2014, *ApJ*, 783, 134
Franchini, A., Sesana, A., & Dotti, M. 2021, *MNRAS*, 507, 1458
Goldreich, P., & Tremaine, S. 1979, *ApJ*, 233, 857
Heath, R. M., & Nixon, C. J. 2020, *A&A*, 641, A64
Hopkins, P. F. 2015, *MNRAS*, 450, 53
Hopkins, P. F. 2016, *MNRAS*, 462, 576
Kormendy, J., & Ho, L. C. 2013, *ARA&A*, 51, 511
Lin, D. N. C., & Papaloizou, J. 1986, *ApJ*, 307, 395
Lodato, G., Nayakshin, S., King, A. R., & Pringle, J. E. 2009, *MNRAS*, 398, 1392
Lynden-Bell, D., & Kalnajs, A. J. 1972, *MNRAS*, 157, 1
Moody, M. S. L., Shi, J.-M., & Stone, J. M. 2019, *ApJ*, 875, 66
Muñoz, D. J., Lai, D., Kratter, K., & Mirand, A. R. 2020, *ApJ*, 889, 114
Muñoz, D. J., Miranda, R., & Lai, D. 2019, *ApJ*, 871, 84
Price, D. J. 2007, *PASA*, 24, 159
Price, D. J., Wurster, J., Nixon, C., et al. 2018, *PASA*, 35, e031
Price, D. J., Wurster, J., Nixon, C., et al. 2017, PHANTOM: Smoothed Particle Hydrodynamics and Magnetohydrodynamics Code, Astrophysics Source Code Library, ascl:1709.002
Quinlan, G. D. 1996, *NewA*, 1, 35
Ragusa, E., Lodato, G., & Price, D. J. 2016, *MNRAS*, 460, 1243
Roedig, C., Sesana, A., Dotti, M., et al. 2012, *A&A*, 545, A127
Sesana, A., Haardt, F., & Madau, P. 2007, *ApJ*, 660, 546
Shakura, N. I., & Sunyaev, R. A. 1973, *A&A*, 24, 337
Springel, V. 2010, *ARA&A*, 48, 391
Tiede, C., Zrake, J., MacFadyen, A., & Haiman, Z. 2020, *ApJ*, 900, 43